Advanced Materials Interfaces

ADVANCED MATERIALS INTERFACES Open Access

www.advmatinterfaces.de

RESEARCH ARTICLE OPEN ACCESS

Mass Spectrometric Investigation of the Influence of Water Vapour and Oxygen on Gas-Phase Reactions of Aluminium Acetylacetonate

Ilyas Adaköy[1] | Sebastian Grimm[1] | Patrick Hemberger[2] | Nina Gaiser[3] | Thomas Bierkandt[3] | Charlotte Rudolph[1] | Christoph Horn[1] | Niklas Tomasik[1] | Burak Atakan[1]

[1]Institute for Energy and Material Processes–Chair of Thermodynamics, University of Duisburg-Essen, Duisburg, Germany | [2]Laboratory for Synchrotron Radiation and Femtochemistry, Paul Scherrer Institute, Villigen, Aargau, Switzerland | [3]German Aerospace Center (DLR), Institute of Combustion Technology, Stuttgart, Germany

Correspondence: Ilyas Adaköy (ilyas.adakoey@uni-due.de)

Received: 2 February 2026 | **Revised:** 4 April 2026 | **Accepted:** 11 April 2026

Keywords: aluminium acetylacetonate | different carrier gases | gas-phase reactions | MOCVD | oxygen | photoelectron photoion coincidence spectroscopy | VUV single-photon ionization | water vapour

ABSTRACT

The controlled synthesis of aluminium oxide (Al_2O_3) thin films by metal–organic chemical vapour deposition (MOCVD) critically depends on the gas-phase decomposition behaviour of metal–organic precursors. Aluminium acetylacetonate ($Al(acac)_3$) is widely used owing to its low toxicity and thermal stability; however, its gas-phase chemistry in the presence of reactive carrier gases such as water vapour and oxygen remains incompletely understood. Here, we present an in-situ mass spectrometric investigation of the gas-phase decomposition of $Al(acac)_3$ using vacuum ultraviolet (VUV) synchrotron radiation coupled with double imaging photoelectron photoion coincidence spectroscopy (i^2PEPICO). Temperature-dependent spectra were recorded in humid ($Ar+H_2O$) and oxygen-containing carrier gas environments, enabling identification of key decomposition products and intermediates. In the presence of water vapour, $Al(acac)_3$ decomposes at lower temperatures than under inert conditions, consistent with a water-mediated weakening of the Al–acetylacetonate bond. This pathway enhances the formation of acetylacetone and acetone, while suppressing characteristic intermediates. In contrast, oxygen exhibits a fundamentally different behaviour: the precursor signal remains nearly constant over a broad temperature range. Only above 700 K does oxygen promote alternative gas-phase decomposition routes. These results highlight the distinct, non-equivalent roles of water vapour and oxygen in MOCVD and their impact on deposition kinetics.

1 | Introduction

Thin aluminium oxide (Al_2O_3) layers can be synthesized by metal-organic chemical vapour deposition (MOCVD) [1]. The applications for Al_2O_3 layers range from anti-corrosion and permeation barrier coating [2–4], surface enhancement coating [2, 5] to an alternative gate dielectric oxide [6, 7]. MOCVD is a process in which a metal-containing precursor in the gas phase reacts with a surface, resulting in the formation of thin films. Metal β-diketonates are suitable precursors due to their relatively high vapour pressure at moderate temperatures and their thermal stability [8, 9]. A frequently used precursor for MOCVD is aluminium tris(acetylacetonate) ($Al(acac)_3$), which is cheap and non-toxic. [10–18] In MOCVD, understanding the gas phase reactions is crucial as it enables the prediction of the growth rate and composition of the synthesized layers [1, 19–23].

Saraie and co-workers [19] investigated the effects of various atmospheres on the reduced-pressure chemival vapour deposition (CVD) of Al_2O_3 films at low temperatures (473–623 K). The effects of nitrogen, nitrogen/hydrogen, nitrogen/oxygen, and nitrogen/water vapour on the MOCVD of Al_2O_3 were analysed using aluminium triisopropoxide (ATI) as a precursor. The authors emphasize that the Al_2O_3 films are deposited through heterogeneous reactions on the substrate surface and not through homogeneous reactions in the gas phase. The deposition rate was largely increased by oxygen. Water vapour also provided a higher deposition rate, even more significant than oxygen [19]. Ciliberto et al., [21]. demonstrated the influence of different carrier gases on the synthesis of aluminium oxide coatings using MOCVD. They investigated aluminium tris-dipivaloylmethanate as a precursor and argon, oxygen, and argon + water vapour were utilized as carrier gases. The experiments were carried out in a horizontal hot-wall reactor made of quartz glass with a constant temperature of 873 K. X-ray photoelectron spectroscopy and secondary ion mass spectrometry were employed to analyse the generated aluminium oxide layers. The experiments showed that the deposition rate increased with oxygen as the carrier gas compared to argon. The highest deposition rate was observed in argon saturated with water vapour, suggesting that water vapour plays a crucial role in accelerating the film growth mechanism [21]. Kim and colleagues [22] aimed to investigate the effects of water vapour on the growth rate of aluminium oxide films by low pressure chemical vapour deposition, using $Al(acac)_3$ as a precursor. The authors analysed the thickness and chemical composition of the synthesized aluminium oxide layers, which allowed them to make assumptions about the kinetics of layer growth, film purity, and surface morphology. Kim et al. investigated $Al(acac)_3$ MOCVD between 503 and 823 K and reported that high water-vapor partial pressures yield ligand-free, pure Al_2 O_3 films with smoother surfaces [22]. Furthermore, the growth rate of the layers depends on the concentration of the water vapour, which confirms the results of the other studies using water vapour [19, 21]. Similarly, Fu et al., [23]. investigated the thermal decomposition pathway of zinc acetylacetonate ($Zn(acac)_2$) and proposed a two-step mechanism. Initially, $Zn(acac)_2$ undergoes evaporation and partial hydrolysis, forming Zn(acac)(OH) and acetylacetone (Hacac), with water acting either as solvent or being released as crystal water. In the absence of additional protons, further decomposition proceeds via an intramolecular proton transfer from a methyl group to the Zn–O moiety, forming $Zn(OH)_2$ and a cumulene intermediate. However, in the presence of water vapour, a water-mediated proton transfer pathway becomes accessible, which bypasses the energetically unfavourable four-membered transition state and thus facilitates a faster decomposition reaction. With this work, Fu et al., [23]. demonstrated that water vapour in the gas phase plays a significant role in the decomposition mechanism and can actively influence the reaction pathway. The intramolecular proton transfer was also reported by Rhoten and DeVore [24], who investigated the thermal decomposition of $Al(acac)_3$ with water vapour in the temperature range of 500–900 K with Fourier transform infrared spectroscopy and gas chromatography-mass spectrometry. According to their findings, the proton transfer constitutes a crucial step in the decomposition mechanism of $Al(acac)_3$, forming Al_2O_3 and acetylacetone ($C_5H_8O_2$) when reacting with water vapour. They found that largely pure Al_2O_3 was formed between 600 and 700 K, confirming the studies of Kim et al., [22].

In MOCVD processes, thin film growth is governed by the transport and decomposition of volatile metal–organic precursors in the gas phase. The resulting film properties are highly sensitive to parameters such as temperature and gas atmosphere, highlighting the importance of understanding precursor decomposition pathways and reaction mechanisms [25]. However, no comprehensive investigation of the gas phase reactions was carried out considering different carrier and reactive gases. Several questions remain unanswered, such as why water vapour as a carrier gas results in a smoother layer. Therefore, it is of particular interest to elucidate how the gas phase composition evolves in the presence of reactive carrier gases as a function of temperature, since only species in the gas phase can reach the surface and directly influence Al_2O_3 film growth.

For an inert atmosphere, the gas phase decomposition of aluminium acetylacetonate was investigated by Grimm et al., [26] using vacuum ultraviolet (VUV) synchrotron radiation, which is used as a reference in the present work. Up to 49 gas phase species were identified at very short reaction times, including radicals, hydrocarbons, oxygenated species, and aluminium containing molecules. In the initial decomposition step, aluminium bis(diketo)acetylactonate-H (*m/z* 224) and acetylacetone (*m/z* 100) is formed at temperatures above 600 K. The reaction is triggered by a hydrogen transfer from the CH_3 group of the axial or equatorial acetylacetonate ligand to the second axial or equatorial one, which leads to the cleavage of a metal-oxygen bond and facilitates the detachment of the ligand from the central aluminium atom. [26] The studies by Grimm et al., [26] confirm the findings of Fu et al., [23]. and Rhoten and DeVore [24], showing that the decomposition of $Al(acac)_3$ in an inert atmosphere proceeds with a higher activation energy compared to alternative pathways. This suggests a kinetically hindered process, which is consistent with the observed slow reaction kinetics. Furthermore, various oxygenates like acetylene, acetone, and ketene were detected as major secondary decomposition products. Additionally, species with mass-to-charge ratios *(m/z) of* 210, 186, and *z* 146 were found in the gas phase for the first time. Aiming for a similar approach, we have characterized the gas phase of $Al(acac)_3$ with water vapour and with oxygen as carrier gases in the present work using double imaging photoelectron photoion coincidence spectroscopy (i^2PEPICO) [27] in a quartz glass CVD reactor, but at much longer reaction times, which are near to the ones under typical CVD conditions. VUV synchrotron radiation was used as a soft ionization technique, suitable for MOCVD processes [28, 29], to unambiguously characterize products considering the gas phase reactions, while suppressing dissociative ionization (fragmentation) [26]. The photon energy for ionization is 8.25 and 9.8 eV. First, a series of measurements was carried out with water vapour in argon ($Ar+H_2O$), with the reactor temperature varied from 453 to 698 K. Further, the volume flow of the carrier gas $Ar+H_2O$ was varied at a constant temperature of 648 K. For the investigations with oxygen as the carrier gas, a temperature interval from 453 to 873 K was analysed at a constant volume flow. These measurements were used to generate and analyse temperature-dependent mass spectra for the gas phase reactions of $Al(acac)_3$ with oxygen and Ar + H_2O as carrier gases at CVD relevant residence times of milliseconds.

TABLE 1 | Ionization energies of selected species relevant for this work.

m/z	Formula	Name	IE (eV)
18	H_2O	Water	12.62 [30]
32	O_2	Oxygen	12.33 [31]
42	C_2H_2O	Ketene	9.62 [32]
58	C_3H_6O	Acetone	9.71 [33]
82	C_5H_6O	2-Methlyfuran Acetylallene	8.38 [34] 9.44 [35]
100	$C_5H_8O_2$ $C_5H_{10}O$	Acetylacetone (enol) Acetylacetone (diketo)	8.90 [35] 9.50 [35]
122	$C_8H_{10}O$	2,6-Dimethylphenol	8.05 [36]
164	$C_{10}H_{12}O_2$	Dimethyl-dihydroxodihydropentalene Dimethyl-hydroxo- ketotetrahydropentalene	7.29 [26] 7.55 [26]
225	$Al(C_5H_7O_2)_2^+$	Fragment of $Al(acac)_3$	9.10 [37]
324	$Al(C_5H_7O_2)_3$	Aluminium acetylacetonate	8.17 [37]

2 | Results and Discussion

First, the temperature-dependent influence of water vapour on the $Al(acac)_3$ gas phase signal, and thus concentration, is presented, and the respective mass spectra are shown. Form these, temperature-dependent profiles for pertinent species are calculated and presented. Subsequently, the impact of water vapour, along with the residence time within the reactor, is examined. The results with oxygen are presented analogously, although the oxygen mole fraction was kept constant.

2.1 | Gas Phase Reactions of Aluminium Acetylacetonate With Water Vapour

Photon energies were chosen to enable detection of the chemically relevant species within the limited synchrotron beamtime while keeping photoionization-induced fragmentation low. To rationalize this choice, the ionization energies of pertinent species are summarized in Table 1. Based on the previous study of gas-phase products from $Al(acac)_3$ pyrolysis by Grimm et al., [26], temperature-dependent mass spectra were recorded at 8.25 and 9.8 eV. The lower photon energy (8.25 eV) provides near-threshold ionization for low-ionization energy (IE) species and therefore minimizes fragmentation, but it cannot ionize several relevant products with higher ionization potentials. Consequently, 9.8 eV was additionally employed to extend the detectable species range. The corresponding mass spectra are shown in Figure 1. In both mass spectra at 453 K, the peak intensity at *m/z* 324 corresponding to the precursor $Al(acac)_3$ is the highest one (the carrier gas is not ionized at these photon energies). The mass spectrum with a photon energy of 8.25 eV shows, in addition to the precursor peak, another peak at *m/z* 170, the intensity of which increases with rising temperature. The mass spectrum at photon energy of 9.8 eV and temperature of 453 K shows peaks of the precursor $Al(acac)_3$, $Al(C_5H_7O_2)_2^+$ at *m/z* 225 and acetylacetone at *m/z* 100. According to the work of Grimm et al., [26] $Al(C_5H_7O_2)_2^+$ is a dissociative photoionization fragment. Up to a temperature of 698 K, the intensities of the peaks for $Al(acac)_3$ and its fragment decrease, while the signal of acetylacetone and acetone (*m/z* 58) appears at a temperature of 523 K, indicating the decomposition. Moreover, a small signal at *m/z* 184 appears starting at a temperature of 523 K, and its intensity increases progressively with rising temperature. In the mass spectra recorded in the presence of water in the gas phase, no hydrocarbons (e.g., ketenes) were detected, whereas hydrocarbons were observed under inert conditions. This finding confirms the results by Grimm et al., [26], who showed that hydrocarbons species are formed during pyrolysis of $Al(acac)_3$. Consequently, our gas-phase observations are consistent with the findings of Kim et al., [22]. and with literature reports of ligand-free Al_2 O_3 film growth under humid conditions. A detailed analysis of the mass spectra and the associated peaks is presented in the following section, along with a proposed reaction mechanism in the presence of water.

The thermal decomposition behaviour of β-diketonate precursors strongly depends on temperature, influencing both reaction pathways and product distribution [38]. The temperature dependent intensities are shown in Figure 2. The signal intensities for the peaks are integrated, normalized to the initial signal of $Al(acac)_3$ at 523 K, and plotted as a function of temperature. The solid lines illustrate the signals in pure argon, while the dashed lines represent those with a water vapour mole fraction of 10%. The intensities for *m/z* 324 representing $Al(acac)_3$ initially run parallel to each other until 673 K. From 673 to 698 K, the signal intensity in the environment with 10% water vapour decreases, whereas the signal in the gas phase without water remains constant, implying faster reactions of $Al(acac)_3$ with water at these temperatures.

The acetylacetone signal intensity (at *m/z* 100) without water vapour decreases constantly, while the intensity with H_2O rises up to a maximum value at 673 K. Additionally, the intensity of acetone (*m/z* 58) with 10% water vapour increases from a temperature of 623 K, while the signal without H_2O remains almost constant. Both compounds are decomposition products of $Al(acac)_3$ and reaction products in the reaction with water, as formulated for the first reaction step with water in Equation (1) as reported by Rhoten and DeVore [24]. Obviously, the products

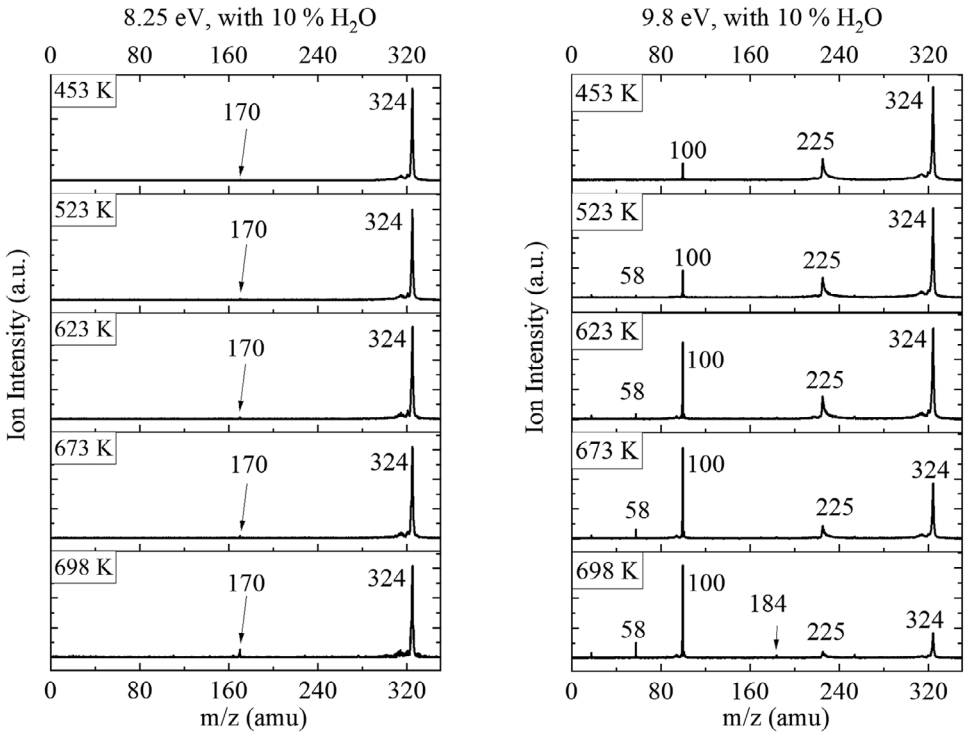

FIGURE 1 | Temperature-dependent photoionization mass spectra with ionization energies of 8.25 and 9.8 eV. The temperature varies from 453 to 698 K. The mole fraction of water vapour in argon is constant and amounts to 10%.

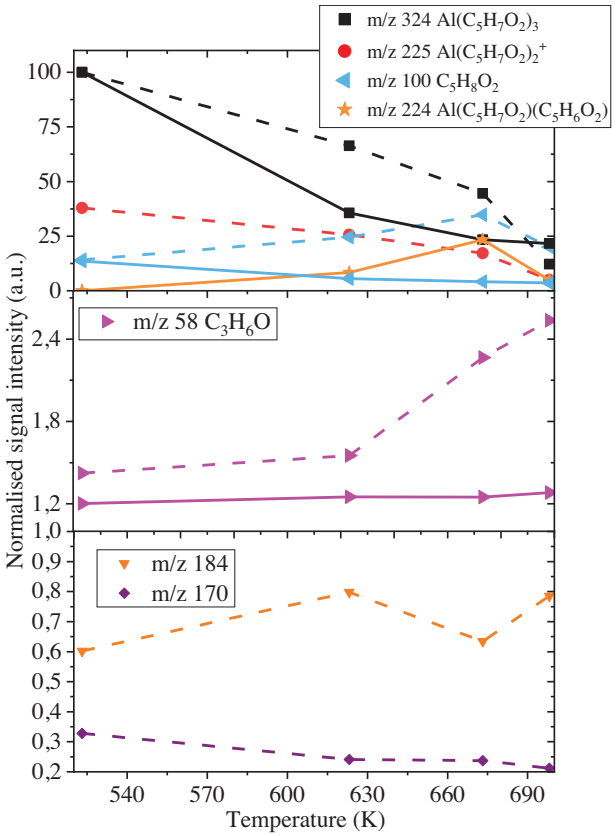

FIGURE 2 | Temperature-dependent species profile. Solid lines represent signals in pure argon as carrier gas, while dashed lines show the intensities in 10% water vapour.

are formed already at lower temperatures in reactions with water, until some consecutive reactions lead to a drop in the intensity of acetylacetone, while further acetone is formed. Especially the reduction in $Al(acac)_3$ concentration in the presence of H_2O is in line with the reported higher growth rates in heterogeneous systems.

$$Al(C_5H_7O_2)_3 + H_2O \rightleftharpoons Al(C_5H_7O_2)_2OH + C_5H_8O_2 \quad (1)$$

Figure 3 illustrates the proposed initial decomposition step of $Al(acac)_3$ in the presence and absence of water vapour, respectively. Although this scheme represents a working hypothesis that will be evaluated in the following by the experimental results, it may ease the understanding of the subsequent discussion. Under inert conditions, the hydrogen transfer occurs from the methyl group of the axial or equatorial acetylacetonate ligand to the second axial or equatorial ligand. This intramolecular process leads to an energetically unfavourable transition state and results in the formation of aluminium bis(diketo)acetylacetonate-H (*m/z* 224) and acetylacetone (*m/z* 100). Similar decomposition pathways have been reported for other β-diketonate precursors, where acetone and related oxygenated species are formed via ligand fragmentation [39, 40]. In contrast, the water molecule may coordinate to the aluminium centre via its oxygen atom, thereby weakening the Al-acetylacetonate (acac) bond. Subsequent proton transfer may lead to dissociation of the acc ligand and formation of *m/z* 242 $Al(C_5H_7O_2)_2OH$ and acetylacetone (*m/z* 100) (see Equation (1) and Figure 3), however mass spectrometric evidence could not be directly observed. Recent studies have shown that water can interact with β-diketone ligands via the carbonyl oxygen, leading to changes in reaction pathways

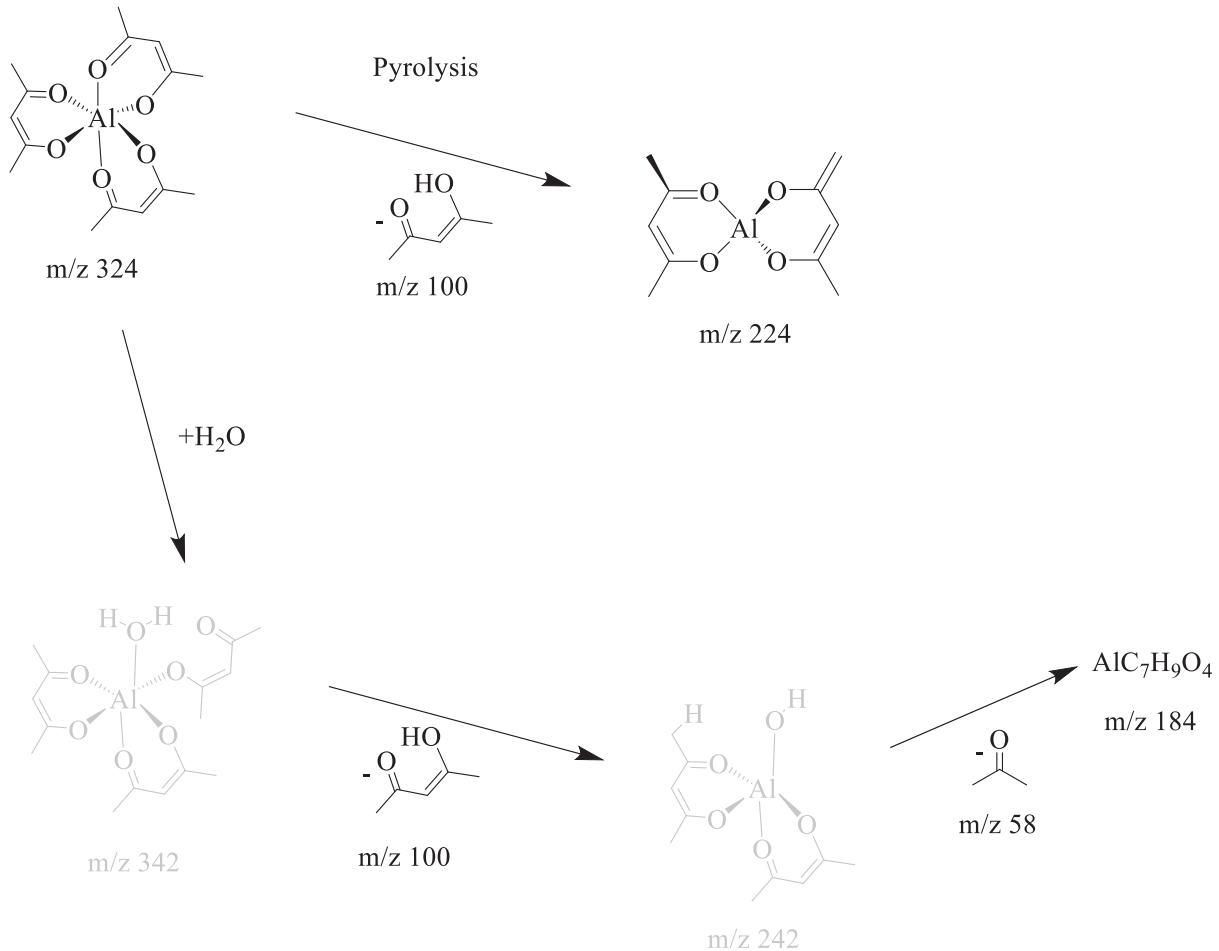

FIGURE 3 | Proposed first decomposition steps with water vapour and without water vapour. Note that both m/z 342 and 242 were not directly observed (given in grey), while the structure of m/z 184 could not be elucidated.

and promoting ligand transformation processes such as proton transfer and ligand dissociation. This supports the proposed mechanism, in which water weakens the metal–ligand bond and facilitates acac removal [41]. The occurrence of the species at *m/z* 184 can only be explained by the presence of water in the gas phase, which accounts for the absence of a detectable signal at *m/z* 242 under these conditions. Rhoten and DeVore [24] demonstrated that acetone (*m/z* 58) can be formed from the species at *m/z* 242, yielding a fragment at *m/z* 184. Figure 2 shows that the intensity of the *m/z* 184 signal increases while the signal attributed to $Al(acac)_3$ decreases. In addition, the signal at *m/z* 58 also increases. This correlation strongly suggests that both acetone (*m/z* 58) and the species at *m/z* 184 originate from *m/z* 242. Within this framework, the species detected at *m/z* 184 may tentatively be assigned to an Al-containing intermediate with the composition $AlC_7H_9O_4$, which has not been reported previously. Consequently, the reaction mechanism in the presence of water is proposed to proceed as illustrated in Figure 3. Since the intermediate at *m/z* 224 is avoided under humid conditions, the decomposition of the precursor proceeds more rapidly compared to that in an inert atmosphere, resulting in higher amounts of decomposition products such as acetylacetone and acetone. Moreover, the mechanism suggests that the enhanced deposition rate is largely attributed to changes in gas-phase reaction kinetics induced by the presence of water vapour.

To substantiate the proposed mechanism with further evidence, Figure 2 also displays the temperature-dependent species profile of *m/z* 224 and *m/z* 225. In the absence of water, a distinct signal at *m/z* 224 corresponding to aluminium bis(diketo)acetylacetonate-H ($Al(C_5H_7O_2)(C_5H_6O_2)$), is observed at temperatures above 600 K, consistent with the findings of Grimm et al., who also determined its I to be 6.64 eV [26]. Under humid conditions, however, *m/z* 224 is not detected at any temperature. Instead, a signal, at *m/z* 225 ($Al(C_5H_7O_2)_2^+$) appears in the presence of water vapour. Furthermore, Figure 1 shows that $Al(C_5H_7O_2)_2^+$ is only detected at a photon energy of 9.8 eV. The observation of m/z 225 as a prominent fragment ion under photoionization conditions strongly suggests its origin from $Al(C_5H_7O_2)_3$ (m/z 324). The complete absence of the corresponding dimer-related signal $Al(C_5H_7O_2)(C_5H_6O_2)$ (m/z 224) under humid conditions suggests that the intramolecular H-transfer pathway required for its formation is suppressed in the presence of water. Instead, the data are consistent with a water-assisted decomposition route that promotes acetylacetonate ligand cleavage.

These gas-phase trends agree with literature reports on $Al(acac)_3$ decomposition and deposition under humid conditions. For example (e.g.), Kim et al., [22]. observed an earlier onset of precursor decomposition and an increased deposition rate in the presence of water and reported the formation of ligand

-free Al_2O_3 films under those conditions. In the present work, the absence of ketenes and other hydrocarbon fragments under humid conditions is consistent with more efficient ligand removal pathways in the gas phase.

Importantly, thin-film properties were not measured in this study; any implications for film composition or morphology are therefore based on gas-phase speciation and comparison with the literature. Furthermore, the increased acetylacetone signal in the presence of water vapor is consistent with the mechanism proposed by Rhoten and DeVore [24] (see Equation (2)), supporting the interpretation above.

$$2Al(C_5H_7O_2)_3 + 3H_2O \rightarrow Al_2O_3 + 6C_5H_8O_2 \quad (2)$$

The signal at m/z 170 is only observed under humid conditions. As shown in Figure 2, its normalized intensity decreases up to ~673 K, indicating that it is associated with the low- to intermediate-temperature chemistry in the presence of water. Notably, m/z 170 is detected at 8.25 eV, whereas a neighbouring signal at m/z 184 is only observed at 9.8 eV; however, this photon-energy dependence alone does not allow a unique compositional assignment because both ionization-threshold effects and dissociative ionization can shape the observed mass spectrum. At present, we therefore refrain from assigning a specific structure to *m/z* 170. The signal may originate from an oxygenated, water-specific reaction product and could involve Al-containing fragments, but contributions from fragmentation of larger precursor-related species cannot be excluded. A conclusive identification and mechanistic interpretation would require dedicated mass-selected i^2PEPICO threshold photoelectron spectra (cf. ref. [27]), and complementary experiments (e.g., isotopic labelling), which are beyond the scope of the present work.

After measuring and analysing the temperature-dependent mass spectra, the influence of the water mole fraction in the gas phase was investigated as a function of residence time and is summarized in Figure 4 for the signals of $Al(acac)_3$, acetylacetone (*m/z* 100), and acetone (*m/z* 58). The reactor temperature is kept constant at 648 K, because a relatively high degree of conversion was obtained in the previous experimental series, without having a total precursor depletion. The residence times varied between circa (ca.) 52 and 90 ms. Without water, the integrated $Al(acac)_3$ signal falls rapidly with residence time and remains almost constant for longer residence times. For mole fractions of 5% and 10%, the intensity is halved with increasing dwell time, seemingly confirming that water vapour in the gas phase accelerates the precursor´s reaction. But the signal for 2.5% H_2O is notable compared to the others, as an increase can be observed with increasing residence time. This could be explained by some consecutive reaction leading to the formation of $Al(acac)_3$, perhaps of some reaction product reacting back with acetylacetone, as formulated in Equation (2). Thus, the acetylacetone signal must be regarded.

For acetylacetone it is seen that the signal levels increase with the water concentration, speeding up the reaction, while depletion reactions of $Al(acac)_3$ are obviously slow at this temperature. Without water, the signal of acetylacetone decreases until a dwell time of 63 ms, after which it is slightly increasing until 75 ms and decreasing afterward. At a water mole fraction of 5%, the initially constant signal starts to drop after 63 ms. The integrated signal intensity at 10% H_2O increases up until 70 ms, then drops to a value of 9, which remains constant until the end. As with $Al(acac)_3$, a clear increase in the integrated signal can be observed for 2.5% H_2O from a residence time of 70 ms.

The signal intensity of acetone without water increases between 63 and 68 ms, after which the intensity remains almost constant. For a 10% water mole fraction, the integrated signal changes slightly, falling up until 65 ms and then rising to a constant intensity. With 5% water, the intensity increases up until 55 ms, then drops linearly to the original value. The integrated signal for a mole fraction of 2.5% initinally drops until 57 ms and remains constant for longer residence times. For most water mole fraction ranges, the time dependences differ significantly from the ones of acetylacetone or $Al(acac)_3$, so that they are not solely formed from it and surface reactions could be involved. The results of the flow variation experiments confirm both, our data and previous findings. Water vapour clearly promotes the decomposition and deposition of the precursor, particularly at tempeatures above 650 K. With an increasing water vapour mole fraction, the signals corresponding to acetylacetone and acetone increase, while the $Al(acac)_3$ signal decreases accordingly.

2.2 | Gas Phase Reactions of Aluminium Acetylacetonate With Oxygen

Once the temperature-dependent mass spectra of the gas phase of $Al(acac)_3$ in water vapour and argon have been investigated, the temperature dependent influence of 10% oxygen in the gas phase is examined, as illustrated in Figure 5 for the same two photon energies of 8.25 and 9.8 eV. In the mass spectra at 8.25 eV, no signals except the ones for the precursor $Al(acac)_3$ can be recognised up to a temperature of 673 K. The signal intensity at *m/z* 164 representing $C_{10}H_{12}O_2$ increases up to a temperature of 873 K. At 873 K, the mass spectrum shows various hydrocarbons, namely (i.e.) $C_5H_{10}O$ (*m/z* 82), $C_8H_{10}O$ (*m/z* 122), $C_{11}H_{14}$ (*m/z* 146), $C_{10}H_{12}O_2$ (*m/z* 164), *m/z* 170, and $Al(acac)_3$ (*m/z* 324).

The mass spectra at an IE of 9.8 eV shows a peak for the precursor at *m/z* 324, the characteristic peak for the dissociative ionization of the precursor (*m/z* 225), acetylacetone (*m/z* 100), and acetone (*m/z* 58) at the lowest temperature of 453 K. At 773 K, further characteristic peaks of hydrocarbons appear, which were previously assigned by Grimm et al., [26], i.e. C_2H_2O or C_3H_6 (*m/z* 42), acetone (*m/z* 58), C_5H_6O (*m/z* 82), acetylacetone (*m/z* 100), $C_8H_{10}O$ (*m/z* 122), $C_{10}H_{12}O_2$ (*m/z* 164), DI of $Al(acac)_3$ (*m/z* 225) and $Al(acac)_3$ (*m/z* 324). The signal intensities of these peaks increase up to a temperature of 873 K, while the intensity for *m/z* 324 and *m/z* 225 decreases.

Figure 6 shows the temperature-dependent normalized intensities for experiments with 10% O_2 in the gas phase (dashed lines) and for pure Ar (solid lines). All signals were normalized to the $Al(acac)_3$ signal at the lowest temperature, where conversion is expected to be minimal. In pure Ar, the $Al(acac)_3$ signal decreases with increasing temperature and approaches a low, nearly constant level above ~810 K.

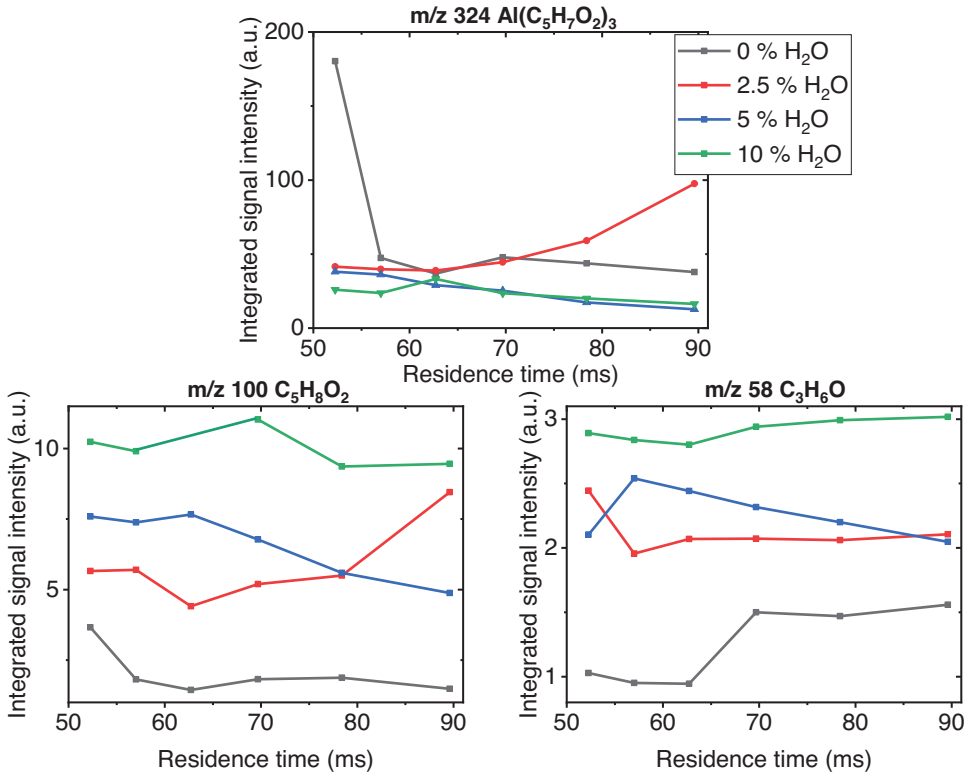

FIGURE 4 | Variation of the mole fraction of water vapour and the residence time in the reactor: Integrated intensities of the signals $Al(acac)_3$, acetone, and acetylacetone from the mass spectra. The water mole fractions are 0%, 2.5%, 5%, and 10%, shown in black, red, blue, and green, respectively. The temperature within the reactor is kept constant at 648 K.

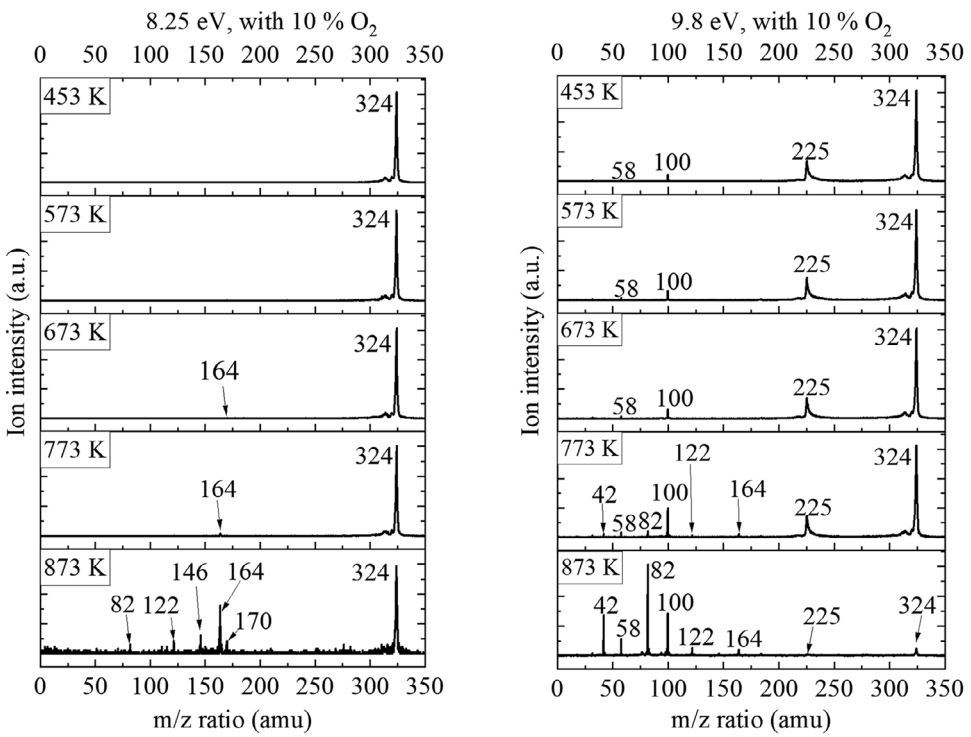

FIGURE 5 | Temperature-dependent photoionization mass spectra with ionization energies of 8.25 and 9.8 eV. The temperature varies from 453 to 873 K. The mole fraction of oxygen is constant and amounts to 10%.

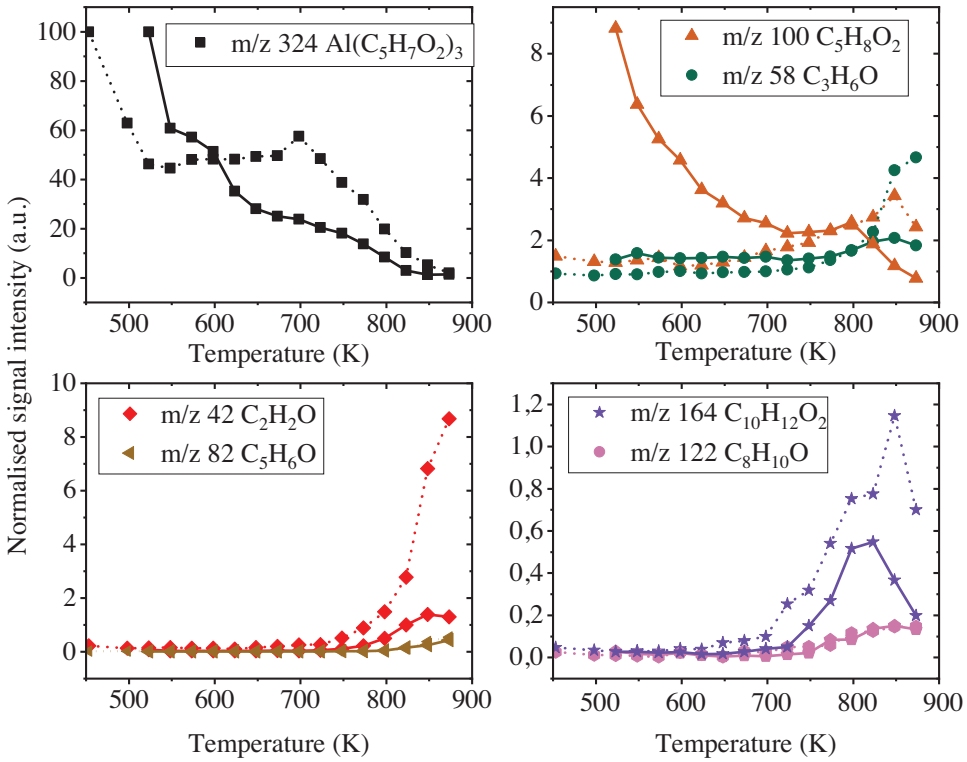

FIGURE 6 | Temperature dependent species profile of various gas-phase species with a mole fraction of 10% oxygen (dashed lines) and pure argon (solid lines).

In the presence of 10% O_2, the $Al(acac)_3$ signal initially decreases more rapidly, but then remains approximately constant between ~510 and ~690 K at a higher level than in Ar. This non-monotonic behaviour indicates that the apparent precursor signal is affected by additional processes under oxidizing conditions. While oxygen has been reported to increase deposition rates in related MOCVD studies (e.g., Ciliberto et al., [21]), a direct one-to-one relation between deposition rate and gas-phase $Al(acac)_3$ signal cannot be inferred from the present data. The observed stabilization could arise from O_2-involving pathways that partially regenerate $Al(acac)_3$ from reactive fragments and/or from heterogeneous contributions such as adsorption–desorption equilibria at reactor surfaces. At present, this interpretation remains speculative because no corresponding intermediates can be identified from the available spectra.

The measured signal intensities for *m/z* 122 show no significant differences for the two conditions. The integrated intensities for the species *m/z* 164 are nearly parallel, with the signal in the presence of oxygen exhibiting higher values.

Acetone (*m/z* 58) shows no significant differences up to a temperature of 820 K. Beyond 820 K, the integrated intensity with oxygen as carrier gas increases significantly compared to the signal without oxygen. This suggests that the formation of acetone is favoured in oxygen-rich gas phase from this temperature onward.

A clear difference between the measured values can be recognized for acetylacetone (*m/z* 100). In pure argon, there is a drop in the signal intensity starting at high levels, which can be recognized over the entire temperature range. In contrast, with oxygen in the gas phase, a slight increase of the low intensity signal can be observed up to a temperature of 820 K.

No differences are evident in the data for *m/z* 82. For ketene *m/z* 42, the integrated intensities are initially similar, but above ~700 K the signal increases more strongly in the presence of O_2 than in pure Ar. This trend is consistent with additional oxygen-assisted high-temperature pathways that enhance ketene formation (e.g., via oxidation of precursor-derived fragments). In contrast, below ~700 K the gas-phase signals do not show clear evidence for an oxygen-induced acceleration of precursor decomposition.

The comparatively stable $Al(acac)_3$ signal in the presence of O_2 suggests that the observed gas-phase signal is influenced by additional processes under oxidizing conditions. One possible explanation is an increased contribution of heterogeneous effects (e.g., adsorption–desorption equilibria and/or surface-mediated consumption of adsorbed precursor), which could be consistent with the enhanced deposition rates reported in oxygen-containing MOCVD environments (e.g., Saraie et al., [19]). However, the present experiment does not provide direct evidence (e.g., surface diagnostics or reactor-material variations) to quantify or unambiguously separate surface and gas-phase contributions; therefore, this interpretation remains tentative. Above ~700 K, the oxygen case shows pronounced changes in several signals (Figure 6), indicating that additional high-temperature reaction channels become important. In this regime, gas-phase oxidation chemistry is expected to play a larger role,

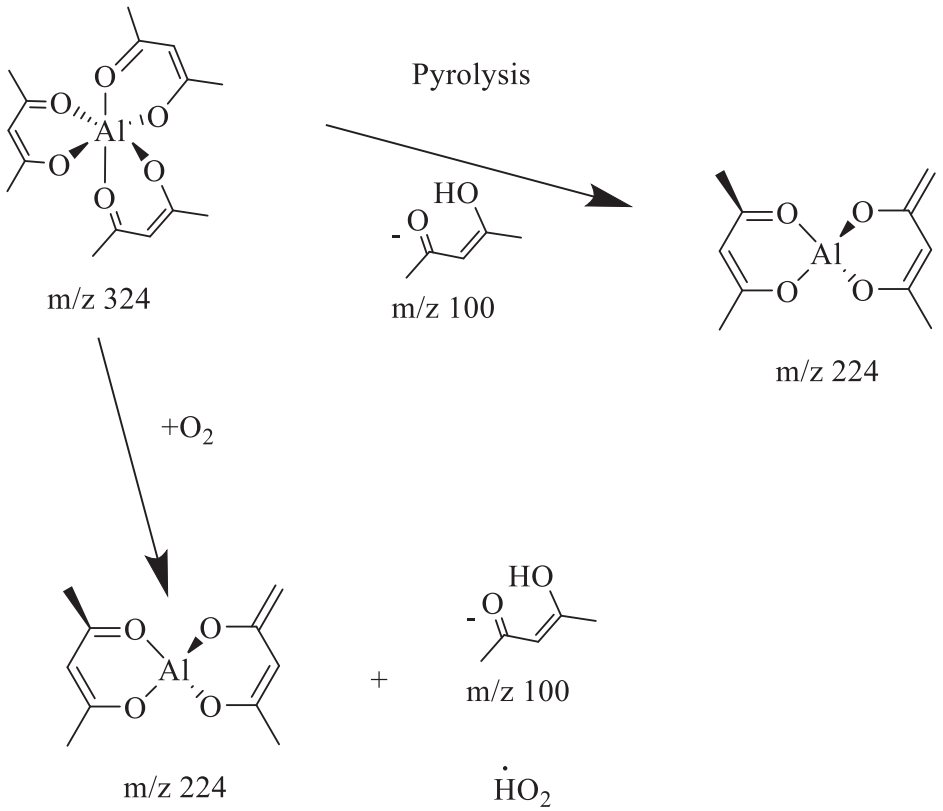

FIGURE 7 | Proposed initial reaction step of aluminium acetylacetonate in the gas phase with a mole fraction of 10% oxygen, starting at 700 K.

consistent with literature on oxygen-assisted decomposition of metal–organic precursors (e.g., Ciliberto et al., [21]). Figure 7 illustrates a plausible oxygen-initiated step, i.e. H abstraction from a methyl group on an acetylacetonate ligand, which would produce HO_2 and an Al-containing radical fragment along with acetylacetone. This mechanistic proposal is illustrative and remains speculative, as characteristic intermediates (e.g., HO_2) cannot be unambiguously identified in the present dataset. This pathway bypasses the energetically unfavourable six-membered transition state associated with the intramolecular proton transfer observed in the unimolecular decomposition. Such a pathway could lower the effective barrier relative to unimolecular decomposition and thereby enhance overall precursor conversion under oxidizing conditions.

The absence of a detectable *m/z* 224 signal may be rationalized by the different temperature windows of intermediate formation and oxygen-assisted chemistry. Under inert conditions, Grimm et al., [26] reported a maximum of the *m/z* 224 intermediate around 660 K. If oxygen-initiated pathways become significant mainly above ~700 K in our experiments, this intermediate may already have been consumed by subsequent unimolecular decomposition and/or further reactions before the oxygen-assisted chemistry becomes prominent, which could explain why it is not observed here.

In comparison to reactions conducted in the presence of water vapour, it becomes evident that hydrocarbons and ketenes are detected when oxygen is present. This observation may explain why only water may promote smoother and ligand-free Al_2O_3 films. Oxygen appears to promote faster reaction pathways and to induce precursor decomposition at a lower temperature than under inert conditions.

3 | Conclusion

The present investigation establishes a mechanistic framework for understanding the influence of water vapour and oxygen on the gas-phase decomposition of $Al(acac)_3$, one of the most widely applied MOCVD precursors for Al_2O_3 thin films. Using temperature- and residence-time-resolved synchrotron-based mass spectrometry, we demonstrate that the two reactants exert fundamentally different effects on the precursor chemistry. Water vapour weakens the Al-acac bond, thereby accelerating the decomposition of $Al(acac)_3$ and preventing the formation of the unfavourable intramolecular proton transfer. As a result, ligand elimination occurs more efficiently, leading to the formation of larger amounts of acetylacetone and acetone, while preventing the appearance of intermediate aluminium–diketonate products. Moreover, no ketene species were detected, which are typically observed under inert conditions. This mechanistic picture provides a molecular-level explanation for previously observed improvements in deposition rate and layer purity when water vapour is introduced during MOCVD, while the increased surface smoothness may be a surface reaction-diffusion effect.

By contrast, oxygen exhibits a two-stage influence. At temperatures below ~700 K, the $Al(acac)_3$ signal does not decrease in the same way as in inert atmospheres but instead remains

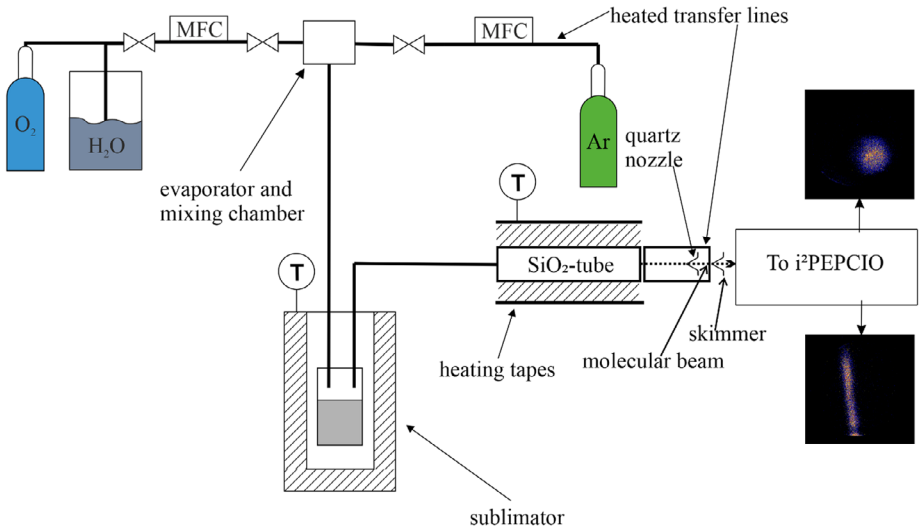

FIGURE 8 | Schematic sketch of the experimental setup. After passing through the flow reactor, the molecular beam is ionized and analysed using i^{2}PEPCIO.

essentially constant over a wide range. This behaviour is consistent with additional O_2 -involving processes that affect the apparent precursor signal, e.g. through partial stabilization and/or reformation of $Al(acac)_3$ from reactive fragments, and/or through heterogeneous contributions such as adsorption–desorption equilibria. Such effects may contribute to the apparent discrepancy between the comparatively stable gas-phase $Al(acac)_3$ signal and the enhanced deposition rates reported for oxygen-containing MOCVD environments. However, the present data do not allow us to distinguish unambiguously between gas-phase and surface-mediated contributions. At higher temperatures, oxygen clearly promotes additional gas-phase decomposition pathways, leading to ketene and oxygenated aromatic/aliphatic species, highlighting the complexity of oxygen-driven chemistry at elevated temperatures.

Taken together, these results underline that the choice of reactive co-gases can be used to steer precursor decomposition pathways under MOCVD-relevant conditions. Water vapor shifts the gas-phase chemistry toward earlier precursor conversion and increased formation of acetylacetone/acetone while suppressing ketene formation, consistent with more efficient ligand-removal pathways and with literature reports of improved film purity under humid conditions. Oxygen, in contrast, shows a stronger temperature dependence: in the intermediate-temperature range, the largely unchanged *m/z* 122 signal and the nearly parallel *m/z* 164 trends (with higher intensities in the presence of O_2) are consistent with additional O_2 -involving channels and/or an increased contribution of heterogeneous effects, but the underlying mechanism cannot be resolved from the present data. At higher temperatures, O_2 clearly promotes additional gas-phase decomposition pathways. From a process perspective, these findings suggest that controlled addition of water vapor can be a practical lever to suppress hydrocarbon by-products, whereas oxygen should be adjusted with care—particularly when operating in temperature windows where undesired oxidation-driven side chemistry becomes significant. Further targeted experiments (e.g., isotope labelling and mass-selected i^{2}PEPICO analysis) are needed to translate these qualitative mechanistic insights into predictive kinetic models.

4 | Experimental Section

All experiments were performed at the vacuum ultraviolet (VUV) beamline [42] at the Swiss Light Source (SLS) of the Paul Scherrer Institute (PSI) in Switzerland. The reactor and diagnostic setup remained unchanged for all measurements; only the mode of reactant dosing was varied, with oxygen introduced as a gas, whereas water vapour was supplied via a separate evaporation unit. Aluminium acetylacetonate was placed in a stainless steel-bubbler immersed in an oil bath acting as a sublimator. Argon was flowed through the bubbler and was saturated with $Al(acac)_3$ (see Figure 8). To ensure isothermal sublimation conditions, the oil bath was monitored with a temperature controller. A silicon dioxide (SiO_2) tube, used as the CVD reactor, had a total length of 600 mm, an inner diameter of 8 mm, and a heated length of 500 mm. The reactor was heated using electrical heating tapes to maintain isothermal conditions along the reactor length. At the reactor outlet, a heated transfer line was installed, extending over the quartz nozzle to prevent condensation and ensure efficient transport of the reaction products to the downstream diagnostics. The pressures inside the reactor and sublimator were set to 100 mbar. An evaporation temperature of 453 K was set. Assuming a saturated gas phase, the mole fraction of $Al(acac)_3$ at the reactor inlet is 4.155×10^{-4}. Owing to uncertainties in the vapor-pressure data, the temperature stability of the sublimator, and potential deviations from ideal saturation, the $Al(acac)_3$ mole fraction is estimated to be uncertain by approximately ±25%. This uncertainty acts primarily as a multiplicative factor on the absolute precursor concentration and thus on the absolute signal levels. The present analysis, however, focuses on temperature-dependent relative trends and normalized signal intensities rather than absolute concentrations. Moreover, the short-term stability of the precursor delivery during an individual temperature sweep is expected

TABLE 2 | Measurement Series for flow variation experiments.

Measurement Series	x_{H2O} [-]	Volume flow range [sccm]
1	0.1	700–1200
2	0.05	700–1200
3	0.025	700–1200
4	0	700–1200

to be significantly higher due to active temperature control of the sublimator. Therefore, the stated uncertainty is not expected to affect the main temperature-dependent trends discussed here.

The reactor temperature was monitored by external thermocouples attached to the reactor wall. Based on the accuracy of the temperature controller, thermocouple calibration, and potential radial temperature gradients, the uncertainty of the absolute reactor temperature is estimated to be ±5 K.

For the series of measurements with water vapour as the carrier gas, a mixing chamber functioning as an evaporator (Controlled Evaporator Mixer manufactured by Bronkhorst) was utilized. Liquid water was fed into the chamber, mixed with argon (99,9999% purity) to form an aerosol, and then vaporised. The mass flows of both water vapour and argon were delivered by Coriolis flowmeters (CFM), allowing precise control over the amount of water and argon. A constant mole fraction of water in argon (x_{H2O} = 0.1) was maintained with a total flow rate of 1000 standard cubic centimtres per minute (sccm). Based on the accuracy specifications of the Coriolis flow meters and the evaporator system, the uncertainty of the water mole fraction is estimated to be within ±5% relative. The temperature within the reactor was varied (T-scan), starting from 453 K, followed by 523, 623, 673, and 698 K. After completing the T-scan, experiments were conducted in which the volume flow and the mole fraction of the water vapour were varied (flow-variation). The reactor temperature is kept constant at 648 K. For clarity, the resulting series of measurements are shown in Table 2. The volume flow of the gas mixture was varied within the range of 700–1200 sccm in increments of 100 sccm. The mole fractions were kept constant by adjusting the mass flows of the carrier gas and the water vapour in each case. This set of experiments aimed to investigate the influence of the amount of water vapour and the effect of the residence time inside the reactor. The residence time can be determined by the reactor geometry and volume flow rate.

The set-up was slightly modified for the series of measurements with oxygen as the carrier gas. Argon flows through the sublimator, mixing with the gaseous precursor. Oxygen was then added to the mixture via a three-way valve. The temperature was varied by 25 K increments, starting from 498 K up to 873 K. The oxygen experiments were extended to 873 K to probe the high-temperature regime under oxidizing conditions; as shown in Figure 6, several signals continue to change significantly above ~700 K, indicating an evolving product distribution. Comparisons between the O_2- and H_2O-containing atmospheres are therefore primarily made within the overlapping range of 453–698 K. The oxygen mole fraction was kept constant at x_{O2} = 0.10 at a total flow rate of 1000 sccm controlled by mass flow controllers (MFCs). Analogous to the water-vapor experiments, the uncertainty in x_{O2} is estimated to be within ±5% (relative). An oxygen mole fraction of 10% was selected to represent a typical oxidizing environment for oxide MOCVD and to enable a controlled comparison of reaction pathways across inert, oxygen-containing, and water-containing atmospheres. Under the present conditions, O_2 is in large excess relative to the $Al(acac)_3$ feed (factor ca. 240); accordingly, the focus of this study is a qualitative comparison between atmospheres rather than establishing a quantitative dependence on oxygen concentration.

After passing through the reactor, the gas mixture flowed through a quartz nozzle attached to the reactor outlet, where it expanded into a vacuum and reached a pressure of 8.3×10^{-6} mbar. The resulting molecular beam was subsequently collimated by a skimmer before entering the ionization region. Ionization was performed using VUV synchrotron radiation, at which point the pressure was 1.7×10^{-6} mbar. The measurement data recorded in this manner were then analysed using i^{2}PEPICO. In all experiments, the ionization energies were set to 8.25 and 9.8 eV. The conditions were set to achieve a good mass resolution (space focus), enabling better distinction between neighbouring masses. A more detailed description of this methodology can be found in the literature [43, 44]. From the temperature-dependent mass spectra of the T-scan, integrated signal intensities of the peaks can be plotted as a function of temperature. The flow-variation experiments allow the visualization of integrated signal intensities from the mass spectra as a function of the dwell time. Both methods facilitate drawing conclusions about changes in the concentration of relevant species within the reactor.

Author Contributions

Ilyas Adaköy: investigation, formal analysis, visualization, writing – original draft **Sebastian Grimm**: investigation, formal analysis; **Patrick Hemberger**: investigation, resources, writing – review & editing; **Thomas Bierkandt**: investigation, resources, writing – review & editing; **Nina Gaiser**: investigation, resources, writing – review & editing; **Charlotte Rudolph**: investigation; **Christoph Horn**: investigation; **Niklas Tomasik**: investigation; **Burak Atakan**: conceptualization, methodology, supervision, writing – review & editing, project administration, funding acquisition.

Acknowledgements

We thank the German Research Foundation (DFG) for financial support under contract 399583933. The measurements have been performed at the VUV beamline of the Swiss Light Source, at the Paul Scherrer Institute in Villigen, Switzerland. Open access funding enabled and organized by Projekt DEAL.

Open access funding enabled and organized by Projekt DEAL.

Conflicts of Interest

The authors declare no conflict of interest.

Data Availability Statement

The data that support the findings of this study are available from the corresponding author upon reasonable request.

References

1. A. C. Jones and M. L. Hitchman, eds., *Chemical Vapour Deposition: Precursors, Processes and Applications* (RSC Publishing, 2009), https://doi.org/10.1039/9781847558794.

2. S. Zhang, L. Zheng, G. Wei, et al., "Structural investigation of Al_2O_3 coatings by PECVD With a high deposition rate," *International Journal of Applied Ceramic Technology* 16, no. 4 (2019): 1356–1363, https://doi.org/10.1111/ijac.13221.

3. A. Michau, Y. Gazal, F. Addou, et al., "Scale up of a DLI-MOCVD Process for the Internal Treatment of a Batch of 16 Nuclear Fuel Cladding Segments With a CrCx Protective Coating," *Surface and Coatings Technology* 375 (2019): 894–902, https://doi.org/10.1016/j.surfcoat.2019.06.101.

4. D. Samelor, L. Baggetto, R. Laloo, et al., "Amorphous Alumina Films Efficiently Protect Ti6242S Against Oxidation and Allow Operation Above 600°C," *Materials Science Forum* 941 (2019): 1846–1852, https://doi.org/10.4028/www.scientific.net/MSF.941.1846.

5. R. Tu, Y. Yuan, L. Guo, et al., "Synthesis of Al_2O_3 Coatings on Ti(C,N)-Based Cermets by Microwave Plasma CVD Using $Al(acac)_3$," *International Journal of Applied Ceramic Technology* 16, no. 6 (2019): 2265–2272, https://doi.org/10.1111/ijac.13255.

6. Z. Li, Y. Xin, Y. Liu, H. Liu, D. Yu, and J. Xiu, "Study of the Annealing Effect on the γ-Phase Aluminum Oxide Films Prepared by the High-Vacuum MOCVD System," *Coatings* 11, no. 4 (2021): 389, https://doi.org/10.3390/coatings11040389.

7. J. Cui, M. G. Kast, and B. A. Hammann, et al., "Aluminum Oxide Thin Films From Aqueous Solutions: Insights From Solid-State NMR and Dielectric Response," *Chemistry of Materials* 30, no. 21 (2018): 7456–7463, https://doi.org/10.1021/acs.chemmater.7b05078.

8. L. G. Hubert-Pfalzgraf, "Metal Alkoxides and β-diketonates as Precursors for Oxide and Non-Oxide Thin Films," *Applied Organometallic Chemistry* 6, no. 6 (1992): 627–643, https://doi.org/10.1002/aoc.590060805.

9. A. Makarenko, S. Trubin, and K. Zherikova, "Breaking Through the Thermodynamics "Wilds" of Metal–Organic Chemical Vapor Deposition Precursors: Metal tris-Acetylacetonates," *Coatings* 13, no. 8 (2023): 1458, https://doi.org/10.3390/coatings13081458.

10. R. Haubner, "The history of hard CVD coatings for tool applications at the University of Technology Vienna," *International Journal of Refractory Metals and Hard Materials* 41 (2013): 22–34, https://doi.org/10.1016/j.ijrmhm.2013.01.012.

11. A. Devi, S. A. Shivashankar, and A. G. Samuelson, "MOCVD of Aluminium Oxide Films Using Aluminium β-Diketonates as Precursors," *Journal de Physique IV (Proceedings)* 12 (2002): 139–146, https://doi.org/10.1051/jp4:20020088.

12. C. Pflitsch, A. Muhsin, U. Bergmann, and B. Atakan, "Growth of Thin Aluminium Oxide Films on Stainless Steel by MOCVD at Ambient Pressure and by Using a Hot-Wall CVD-Setup," *Surface and Coatings Technology* 201 (2006): 73–81, https://doi.org/10.1016/j.surfcoat.2005.10.036.

13. A. Nebatti, C. Pflitsch, B. Curdts, and B. Atakan, "Using the Acetylacetonates of Zinc and Aluminium for the Metalorganic Chemical Vapour Deposition of Aluminium Doped Zinc Oxide Films," *Materials Science in Semiconductor Processing* 39 (2015): 467–475, https://doi.org/10.1016/j.mssp.2015.05.053.

14. S. Li, D. He, X. Liu, S. Wang, and L. Jiang, "Deuterium Permeation of Amorphous Alumina Coating on 316L Prepared by MOCVD," *Journal of Nuclear Materials* 420 (2012): 405–408, https://doi.org/10.1016/j.jnucmat.2011.10.040.

15. A. Ito, R. Tu, and T. Goto, "Amorphous-Like Nanocrystalline γ-Al_2O_3 Films Prepared by MOCVD," *Surface and Coatings Technology* 204 (2010): 2170–2174, https://doi.org/10.1016/j.surfcoat.2009.11.043.

16. T. Goto, "A Review: Structural Oxide Coatings by Laser Chemical Vapor Deposition," *Journal of Wuhan University of Technology-Mater Sci Ed* 31 (2016): 1–5, https://doi.org/10.1007/s11595-016-1319-6.

17. P. Rodriguez, B. Caussat, C. Ablitzer, X. Iltis, and M. Brothier, "Fluidization and Coating of Very Dense Powders by Fluidized Bed Chemical Vapour Deposition," *Chemical Engineering Research and Design* 91 (2013): 2477–2483, https://doi.org/10.1016/j.cherd.2012.11.007.

18. F. A. D. Battaglin, E. S. Prado, L. Caseli, et al., "Films Deposited From Reactive Sputtering of Aluminum Acetylacetonate Under Low Energy Ion Bombardment," *Materials Research* 20 (2017): 926–936, https://doi.org/10.1590/1980-5373-MR-2016-0647.

19. J. Saraie, K. Ono, and S. Takeuchi, "Effects of Various Atmospheres on the Reduced-Pressure CVD of Al_2O_3 Thin Films at Low Temperatures," *Journal of The Electrochemical Society* 136 (1989): 3139–3141, https://doi.org/10.1149/1.2096415.

20. C. Chatfield, J. N. Lindström, and M. E. Sjöstrand, "MICROSTRUCTURE OF CVD—Al_2O_3," *Le Journal de Physique Colloques* 50 (1989), https://doi.org/10.1051/jphyscol:1989545.

21. E. Ciliberto, I. Fragalà, R. Rizza, G. Spoto, and G. C. Allen, "Synthesis of Aluminum Oxide Thin Films: Use of Aluminum Tris-Dipivaloylmethanate as a New Low Pressure Metal Organic Chemical Vapor Deposition Precursor," *Applied Physics Letters* 67 (1995): 1624–1626, https://doi.org/10.1063/1.114960.

22. J. S. Kim, H. A. Marzouk, P. J. Reucroft, J. D. Robertson, and C. E. Hamrin, "Effect of Water Vapor on the Growth of Aluminum Oxide Films by Low Pressure Chemical Vapor Deposition," *Thin Solid Films* 230 (1993): 156–159, https://doi.org/10.1016/0040-6090(93)90509-N.

23. Y. Fu, S. Gledhill, and C.-H. Fischer, "Mechanistic Study of the Gas-Phase Chemistry During the Spray Deposition of Zn(O,S) Films by Mass Spectrometry," *Ultrasonics Sonochemistry* 73 (2021): 105492, https://doi.org/10.1016/j.ultsonch.2021.105492.

24. M. C. Rhoten and T. C. DeVore, "Evolved Gas Analysis Investigation of the Reaction Between Tris(2,4-pentanedionato)aluminum and Water Vapor in Chemical Vapor Deposition Processes To Produce Alumina," *Chemistry of Materials* 9 (1997): 1757–1764, https://doi.org/10.1021/cm960504p.

25. T. A. Kuznetsova, V. A. Lapitskaya, S. A. Chizhik, B. Warcholinski, and A. Gilewicz, "Effect of Atmosphere During Deposition on Zr-Based Coatings," *Advanced Materials Modelling for Mechanical, Medical and Biological Applications* (Springer, 2022), 271–280.

26. S. Grimm, S.-J. Baik, P. Hemberger, et al., "Gas-Phase Aluminium Acetylacetonate Decomposition: Revision of the Current Mechanism by VUV Synchrotron Radiation," *Physical Chemistry Chemical Physics* 23 (2021): 15059–15075, https://doi.org/10.1039/D1CP00720C.

27. A. Bodi, P. Hemberger, D. L. Osborn, and B. Sztáray, "Mass-Resolved Isomer-Selective Chemical Analysis With Imaging Photoelectron Photoion Coincidence Spectroscopy," *The Journal of Physical Chemistry Letters* 4 (2013): 2948–2952, https://doi.org/10.1021/jz401500c.

28. N. Bahlawane, P. A. Premkumar, Z. Tian, X. Hong, F. Qi, and K. Kohse-Höinghaus, "Nickel and Nickel-Based Nanoalloy Thin Films From Alcohol-Assisted Chemical Vapor Deposition," *Chemistry of Materials* 22 (2010): 92–100, https://doi.org/10.1021/cm902454w.

29. Z. Zhang, Y. Pan, J. Yang, Z. Jiang, and H. Fang, "Experimental Study of Trimethyl Aluminum Decomposition," *Journal of Crystal Growth* 473 (2017): 6–10, https://doi.org/10.1016/j.jcrysgro.2017.05.020.

30. P. Linstrom, *NIST Chemistry WebBook, NIST Standard Reference Database Number 69* (National Institute of Standards and Technology, 1997).

31. M. S. Banna and D. A. Shirley, "Molecular Photoelectron Spectroscopy at 132.3 eV: N_2, CO, C_2H_4 and O_2," *Journal of Electron Spectroscopy and Related Phenomena* 8 (1976): 255–270, https://doi.org/10.1016/0368-2048(76)81011-0.

32. B. Niu, D. A. Shirley, and Y. Bai, "High Resolution Photoelectron Spectroscopy and Femtosecond Intramolecular Dynamics of H_2CO^+ and D_2CO^+," *The Journal of Chemical Physics* 98 (1993): 4377–4390, https://doi.org/10.1063/1.464999.

33. E. E. Rennie, A.-M. Boulanger, P. M. Mayer, et al., "A Photoelectron and TPEPICO Investigation of the Acetone Radical Cation," *The Journal of Physical Chemistry A* 110 (2006): 8663–8675, https://doi.org/10.1021/jp0616866.

34. T. Veszprémi, L. Nyulászi, T. Pasinszki, and J. Réffy, "UV Photoelectron Spectroscopy of Furan Derivatives," *Journal of Physical Chemistry A* 110 (2006): 8663–8670.

35. I. Antonov, K. Voronova, M.-W. Chen, et al., "To Boldly Look Where No One Has Looked Before: Identifying the Primary Photoproducts of Acetylacetone," *The Journal of Physical Chemistry A* 123 (2019): 5472–5490, https://doi.org/10.1021/acs.jpca.9b04640.

36. T. Kobayashi and S. Nagakura, "Photoelectron Spectra of Substituted Benzenes," *Bulletin of the Chemical Society of Japan* 47 (1974): 2563–2572, https://doi.org/10.1246/bcsj.47.2563.

37. A. Y. Ustinov, V. I. Vovna, and O. M. Ustinova, "Experimental and Theoretical Investigation of Aluminium, Gallium and Indium Tris-Acetylacetonates Ground, Excited and Ionized States Nature," *Journal of Electron Spectroscopy and Related Phenomena* 88-91 (1998): 103–108, https://doi.org/10.1016/S0368-2048(97)00280-6.

38. K. V. Zherikova, A. M. Makarenko, A. V. Sartakova, and D. P. Pishchur, "Towards the MOCVD's Paradise: Thermodynamics of Phase Transitions of New Scandium Precursors," *The Journal of Chemical Thermodynamics* 189 (2024): 107184, https://doi.org/10.1016/j.jct.2023.107184.

39. S. Grimm, S.-J. Baik, P. Hemberger, T. Kasper, A. M. Kempf, and B. Atakan, "Insights Into the Decomposition of Zirconium Acetylacetonate Using Synchrotron Radiation: Routes to the Formation of Volatile Zr-Intermediates," *Journal of Materials Research* 37 (2022): 1558–1575, https://doi.org/10.1557/s43578-022-00566-6.

40. A. Daher, M. Choudhari, T. Roland, V. De Waele, and S. Daniele, "Zinc β-Diketonates With Donor-Acceptor Ligands: Synthesis and Comprehensive Structural, Thermal, and Photophysical Characterization," *Molecules (Basel, Switzerland)* 30 (2025): 4325, https://doi.org/10.3390/molecules30224325.

41. Y. Ji, W. Luo, and Q. Shi, et al., "Mechanisms of Isomerization and Hydration Reactions of Typical B-Diketone at the Air-Droplet Interface," *Journal of Environmental Sciences* 141 (2024): 225–234, https://doi.org/10.1016/j.jes.2023.04.013.

42. M. Johnson, A. Bodi, L. Schulz, and T. Gerber, "Vacuum ultraviolet beamline at the Swiss Light Source for chemical dynamics studies," *Nuclear Instruments and Methods in Physics Research Section A: Accelerators, Spectrometers, Detectors and Associated Equipment* 610 (2009): 597–603, https://doi.org/10.1016/j.nima.2009.08.069.

43. B. Sztáray, K. Voronova, K. G. Torma, et al., "CRF-PEPICO: Double Velocity Map Imaging Photoelectron Photoion Coincidence Spectroscopy for Reaction Kinetics Studies," *The Journal of Chemical Physics* 147 (2017): 013944, https://doi.org/10.1063/1.4984304.

44. D. L. Osborn, C. C. Hayden, P. Hemberger, A. Bodi, K. Voronova, and B. Sztáray, "Breaking Through the False Coincidence Barrier in Electron–Ion Coincidence Experiments," *The Journal of Chemical Physics* 145 (2016): 164202, https://doi.org/10.1063/1.4965428.